

# RSC Advances



This is an *Accepted Manuscript*, which has been through the Royal Society of Chemistry peer review process and has been accepted for publication.

*Accepted Manuscripts* are published online shortly after acceptance, before technical editing, formatting and proof reading. Using this free service, authors can make their results available to the community, in citable form, before we publish the edited article. This *Accepted Manuscript* will be replaced by the edited, formatted and paginated article as soon as this is available.

You can find more information about *Accepted Manuscripts* in the [Information for Authors](#).

Please note that technical editing may introduce minor changes to the text and/or graphics, which may alter content. The journal's standard [Terms & Conditions](#) and the [Ethical guidelines](#) still apply. In no event shall the Royal Society of Chemistry be held responsible for any errors or omissions in this *Accepted Manuscript* or any consequences arising from the use of any information it contains.

## ARTICLE

# Effects of Template Removal on Both Morphology of Mesoporous Silica Coated Gold Nanorod and Its Biomedical Application

Cite this: DOI: 10.1039/x0xx00000x

Jie Feng<sup>a</sup>, Zhifei Wang<sup>\*.a</sup>, Bin Shen<sup>a</sup>, Liming Zhang<sup>b</sup>, Xia Yang<sup>a</sup>, Nongyue He<sup>\*.b</sup>

Received 00th January 2014,

Accepted 00th January 2014

DOI: 10.1039/x0xx00000x

[www.rsc.org/](http://www.rsc.org/)

Mesoporous silica coated Au nanorods ( $\text{Au}_{\text{rod}}@ \text{SiO}_2$ ) have recently attracted considerable interest in nanomedicine, and the template removal procedure is crucial for the preparation of such hybrid nanostructure. Herein, two kinds of typical extraction solvents ( $\text{NH}_4\text{NO}_3/\text{CH}_3\text{OH}$  and  $\text{HCl}/\text{CH}_3\text{OH}$ ) were separately used to extract the surfactant cetyltrimethylammonium bromide (CTAB) from the obtained  $\text{Au}_{\text{rod}}@ \text{SiO}_2$ . The results show that CTAB molecules could be completely removed from the pores of  $\text{Au}_{\text{rod}}@ \text{SiO}_2$  without damaging the internal Au nanorod by  $\text{NH}_4\text{NO}_3/\text{CH}_3\text{OH}$ , while  $\text{Au}_{\text{rod}}@ \text{SiO}_2$  treated with  $\text{HCl}/\text{CH}_3\text{OH}$  suffered from both poor extraction efficiency and the shape transformation of Au nanorod caused by the selective etching in the presence of oxygen. In addition, the consequent drug loading experiment shows that  $\text{Au}_{\text{rod}}@ \text{SiO}_2$  extracted by  $\text{NH}_4\text{NO}_3/\text{CH}_3\text{OH}$  possesses a larger drug loading capacity with the loading efficiency of 82.5%. Furthermore, the *in vitro* photo-thermal therapy experiment shows that  $\text{Au}_{\text{rod}}@ \text{SiO}_2$  extracted by  $\text{NH}_4\text{NO}_3/\text{CH}_3\text{OH}$  is more efficient in killing the YCC-2 gastric cancer cells as compared with that extracted by  $\text{HCl}/\text{CH}_3\text{OH}$ .

## Introduction

Recently, the development of hybrid nanomaterials with multiple functionalities, such as diagnostic imaging, drug delivery and therapy, has been attracting more attention in the biomedical fields. Compared with pure nanoparticles (NPs), the hybrid nanomaterial can cleverly integrate various properties into unique nanoparticle formulation, and further has potential improvement on the previously established therapeutic and diagnostic regimes.<sup>1</sup> Among various hybrid nanomaterials, mesoporous silica coated Au nanorods ( $\text{Au}_{\text{rod}}@ \text{SiO}_2$ ) have specially stirred up great interest. In this hybrid structure, Au nanorods exhibit intriguing nonlinear optical properties owing to their localized surface plasmon resonances that can be synthetically tuned across a broad spectral range, covering the visible and near-infrared regions by tailoring their aspect ratios (the ratio between the length and diameter). Such splendid plasmon-related property makes Au nanorods be used in both imaging and photothermal conversion-based therapy.<sup>2-5</sup> Meanwhile, mesoporous silica shell (MSS) has also gained much attention due to its unique features, such as large surface area and pore volume, high chemical and thermal stability, excellent biocompatibility, and versatile surface chemistry for further functionalization.<sup>6, 7</sup> Therefore, it can work as “nanocarrier” for the delivery of drugs or other cargos to cells and also be used as the ideal platform for constructing multifunctional materials.

Up to now, the main procedure to fabricate  $\text{Au}_{\text{rod}}@ \text{SiO}_2$  always involves the use of cetyltrimethylammoniumbromide (CTAB), which is first used as stabilizer in the synthesis of Au nanorods, and subsequently as the soft template for the formation of mesoporous silica shell.<sup>8</sup> And in the post-synthesis treatments, CTAB should be efficiently removed to get a more open and hollow pore channel so

as to increase its drug loading capacity. In addition, the residual CTAB is potentially toxic for human system when using  $\text{Au}_{\text{rod}}@ \text{SiO}_2$  as drug carrier. Therefore, how to effectively remove CTAB template is an important issue before its real application as a theranostic platform. So far, numerous methods, including high-temperature thermal-chemical calcinations processes,<sup>9</sup> dialysis,<sup>10</sup> and solvent extraction,<sup>11</sup> have been proposed to remove the template from silica based mesostructured materials. The calcination processes, owing to their aggressive thermal and/or chemical environments, often damage the intrinsic physical-chemical characteristics of the underlying substrate, thus limiting their application in the removal of CTAB from the obtained  $\text{Au}_{\text{rod}}@ \text{SiO}_2$ . The “dialysis” process is time-consuming, and the treatment often requires a large amount of water containing acetic acid, which is neither environmental-friendly nor cost-effective for the real production. Therefore, to the best of our knowledge, solvent extraction is the most effective way to remove CTAB from the silica based mesostructured hybrid NPs.

However, compared with pure silica based mesostructured materials, the effect of solvent extraction on the property of hybrid silica based mesostructured NPs has been reported rarely. As we know, as the core in  $\text{Au}_{\text{rod}}@ \text{SiO}_2$ , Au nanorods have been reported to easily reshape or to suffer from size reduction upon the various conditions such as the treatment with cyanide,<sup>12</sup> oxygen,<sup>13</sup> ferric chloride,<sup>14</sup>  $\text{Cu}^{2+}$  and ascorbic acid in a hot aqueous solution.<sup>15</sup> In order to guarantee its potential efficacy as a theranostic platform, it's crucial for us to find a kind of extraction solvent, which can not only extract all the CTAB molecules from  $\text{Au}_{\text{rod}}@ \text{SiO}_2$ , but also maintain the original shape of both mesoporous silica NPs and internal Au nanorod. Generally speaking, the high efficiency of template removal requires that the suitable solvent not only has the good

accessibility to highly cross-linked regions but also can break the interactions between CTAB and the siliceous mesostructured framework. Therefore, in most cases, the methanol solvent containing cations such as  $H^+$ ,  $NH_4^+$  is most recommended, where CTAB is expected to be removed through both its dissolution in methanol and the ion exchange between  $H^+$  or  $NH_4^+$  and CTAB.

For the reasons mentioned above, herein we comparatively studied the effect of two different extraction solvents ( $NH_4NO_3/CH_3OH$  and  $HCl/CH_3OH$ ) on the efficiency of CTAB removal from the obtained  $Au_{rod}@SiO_2$ . Their effect on both morphology and plasmon-related properties of the obtained  $Au_{rod}@SiO_2$  were emphatically investigated. Then the drug loading experiment was carried out to assess the effect of two extraction solvents on the drug loading capacity. Finally the *in vitro* photo-thermal therapy experiment was implemented to evaluate the photo-thermal therapy (PTT) effect of  $Au_{rod}@SiO_2$  after solvent extraction. These results reported here will lay a solid foundation for the  $Au_{rod}@SiO_2$  based photo-thermal therapy and drug delivery.

## Experimental

### Materials

Gold(III) chloride ( $HAuCl_4 \cdot 3H_2O$ ), cetyltrimethylammonium-bromide (CTAB), silver nitrate ( $AgNO_3$ ), sodium borohydride ( $NaBH_4$ ), sodium hydroxide ( $NaOH$ ), methanol ( $CH_3OH$ ), L-ascorbic acid (AA), and tetraethyloxysilane (TEOS) were purchased from Sinopharm Chemical Reagent Limited Corporation and used as received. 3-aminopropyltriethoxysilane (APTES), polyacrylic acid (PAA, MW=1,800), and DOX in the form of the hydrochloride salt were purchased from Aladdin.  $\alpha$ -mPEG- $\omega$ -amine (MW=10,000) was purchased from Shanghai Yanyi Biotechnology Corporation. Fetal bovine serum (FBS), Dulbecco's modified Eagle's medium, penicillin/streptomycin were purchased from ThermoFisher Scientific. Calcein-AM and propidium iodide (PI) were obtained from Invitrogen. All glassware and Teflon-coated magnetic stirring bars were thoroughly cleaned with aqua regia, followed by copious rinsing with purified water. Water was purified with a Millipore system.

### Synthesis of Au nanorods

Au nanorods were fabricated by a seed-mediated, Ag (I)-assisted growth procedure according to the previous report.<sup>8</sup> The seed solution was prepared as follows: Briefly, 0.25 mL of an aqueous solution of  $HAuCl_4$  solution (0.01 M) was added to 7.5 mL of CTAB solution (0.10 M) in a test tube. The solutions were gently mixed by inversion. The solutions appeared bright brown-yellow in color. Then, 0.6 mL of an aqueous ice-cold  $NaBH_4$  solution (0.01 M) was added all at once, followed by rapid inversion mixing for 2 min. The resulting solution developed a pale brown-yellow color. After that, the test tube was kept in a water bath maintained at 25 °C to obtain stable seed solution. The growth solution was prepared by mixing 285 mL of CTAB (0.1 M), 12 mL of  $HAuCl_4$  (0.01 M) and 1.8 mL of  $AgNO_3$  (0.01 M) together in 500 mL reagent bottle. Another 100  $\mu$ L of HCl (37%, wt) was added into the above solution. Following this step, 1.92 mL of L-ascorbic acid (0.01 M) was added to the resulting solution under gentle stirring, which changed the color of the growth solution from dark yellow to colorless. Finally 0.6 mL of seed solution was added to the resulting solution at 27–30 °C. The color of the solution gradually changed within 10–20 min. The temperature of the growth medium was kept constant at 27–30 °C during the whole procedure.

### Synthesis of $Au_{rod}@SiO_2$

The post mesoporous silica coating of Au nanorods were achieved by a modified stober method. Firstly, 200 mL of as-synthesized Au

nanorods were washed twice with Milli-Q water to remove excess CTAB and redispersed in 100 mL of Milli-Q water. Subsequently, 10 mL of NaOH solution (0.1 M) was added to adjust the pH value to 11, then 0.9 mL of 20% TEOS in methanol solution was added to the resulting solution at the rate of 300  $\mu$ L every 30 min. The mixture was allowed to react at 27 °C for at least 2 days. The resulting  $Au_{rod}@SiO_2$  was washed two times with water and three times with methanol and finally dispersed into 100 mL of methanol.

### The removal of CTAB from the as-synthesized $Au_{rod}@SiO_2$ by HCl/ $CH_3OH$ (denoted as “route A”) or $NH_4NO_3/CH_3OH$ (denoted as “route B”) extraction

The removal of CTAB from the as-synthesized  $Au_{rod}@SiO_2$  was carried out by two different solvent extraction methods. Typically, the removal of CTAB by HCl/ $CH_3OH$  extraction was performed in 0.25 M HCl/ $CH_3OH$  solution at 60 °C. Firstly, 2 mg of as-synthesized  $Au_{rod}@SiO_2$  was added to 5 mL of 0.25 M HCl/ $CH_3OH$  solution. Then the resulting mixture was heated to reflux at 60 °C under stirring. In comparison, the removal of CTAB by  $NH_4NO_3/CH_3OH$  extraction is similar to the above the procedure, except that HCl/ $CH_3OH$  was replaced by 5 mL of methanol solution containing 30 mg of  $NH_4NO_3$ . For the sake of comparison, the extracted  $Au_{rod}@SiO_2$  was taken out and washed by methanol at selected time for both UV-vis and TEM characterization.

### Evaluation of drug loading capacity of $Au_{rod}@SiO_2$ treated with route A or route B

DOX was chosen as a model drug to assess the effect of different extraction solvents on drug loading capacity of the extracted  $Au_{rod}@SiO_2$ . Briefly, 1 mg of the extracted  $Au_{rod}@SiO_2$  was mixed with 1 mL of PBS buffer containing 100  $\mu$ g of DOX and stirred at room temperature for 24 h. Then the supernatant was collected and the residual DOX content was measured by UV-vis measurement at a wavelength of 480 nm. The loading efficiency (LE) is obtained using the following equation:

$$LE(\%) = \frac{DOX_{original} - DOX_{supernatant}}{DOX_{original}}$$

### Preparation of PEGylated $Au_{rod}@SiO_2$

To improve the biocompatibility of  $Au_{rod}@SiO_2$ , their surface was further functionalized with  $\alpha$ -mPEG- $\omega$ -amine group prior to the *in vitro* photo-thermal therapy experiment. Firstly, 5 mg of  $Au_{rod}@SiO_2$  treated by route A or route B was dispersed in 5 mL of methanol, and then 100  $\mu$ L of APTES was rapidly added to the above solution. After 24 h of reaction under room temperature, the APTES functionalized  $Au_{rod}@SiO_2$  (denoted as  $Au_{rod}@SiO_2@NH_2$ ) was obtained by centrifugation at 15,000 rpm for 10 min to remove supernatant, washed with ethanol for four times, and dried under vacuum. After that, polyacrylic acid (PAA, MW=1,800) was further covalently attached to the surface of  $Au_{rod}@SiO_2@NH_2$  using EDC coupling chemistry with the aim to obtain carboxylate-functionalized  $Au_{rod}@SiO_2$  (denoted as  $Au_{rod}@SiO_2@COOH$ ). Briefly, 0.03 g of PAA dissolved in 2 mL of MES buffer (pH =6.0) was first activated with the help of 1 mg of EDC. Then, 5 mg of the obtained  $Au_{rod}@SiO_2@NH_2$  was added into the above solution, and the reaction lasted for 30 min. Next, the resultant was purified by centrifugation and subsequently washed with PBS buffer for at least 3 times. For further PEGylation, 100  $\mu$ L of EDC (10 mg/mL) and 100  $\mu$ L of NHS (10 mg/mL) were separately added to 2 mL of aqueous solution containing 5 mg of  $Au_{rod}@SiO_2@COOH$ . After

activation for 30 min, 1 mL of mPEG<sub>10000</sub>-NH<sub>2</sub> solution (100 mg/mL) was added to the above mixture and kept stirring for overnight. Finally, the PEGylated Au<sub>rod</sub>@SiO<sub>2</sub> (denoted as Au<sub>rod</sub>@SiO<sub>2</sub>@PEG) was collected and washed with distilled water by centrifugation at 15,000 rpm. And the resulting particles were dispersed in distilled water.

### ***In vitro* photo-thermal therapy (PTT) of Au<sub>rod</sub>@SiO<sub>2</sub> treated with route A or route B**

The *in vitro* photo-thermal therapy experiment was further carried out to investigate the cancer killing efficiency of the Au<sub>rod</sub>@SiO<sub>2</sub> treated with two extraction solvents. Firstly, gastric cancer cells YCC-2 were seeded in a 24-well flat culture plate. After incubation overnight to allow cell attachment, the cells were then incubated with 50  $\mu$ L of 1mg/mL PEGylated Au<sub>rod</sub>@SiO<sub>2</sub> in normal DMEM cell medium containing 10% fetal bovine serum (FBS) and 1% penicillin/streptomycin at 37  $^{\circ}$ C in a humidified atmosphere containing 5% CO<sub>2</sub>. After 24 h incubation, free Au<sub>rod</sub>@SiO<sub>2</sub> was removed from the culture medium by rinsing three times with PBS. Cells were then irradiated with an 808 nm optical fiber-coupled diode near-infrared (NIR) Laser at power density of 3 W/cm<sup>2</sup> for 1, 2, 4 min, respectively. After irradiation, the cell viability was assessed by Calcein-AM/propidium iodide double staining as reported method.<sup>16</sup> Cells cultured without the addition of the resulting Au<sub>rod</sub>@SiO<sub>2</sub> at the same time intervals were used as the negative control. Fluorescence microscopic images of stained cells were then taken using an Olympus fluorescent microscope.

### **Characterization**

The morphology and size of both Au nanorods and Au<sub>rod</sub>@SiO<sub>2</sub> were acquired by Transmission Electron Microscopy (TEM). Before the measurement, samples were prepared by drying a drop of dispersion of Au nanorods or Au<sub>rod</sub>@SiO<sub>2</sub> suspension on a carbon-coated copper grid at room temperature and were analyzed using a JEOL JEM 2100 F electron microscope equipped with operating voltage of 200kV. UV-vis spectrum was recorded on a Shimadzu spectrometer spectrophotometer, between 450 and 1000 nm wavelength. And the samples were measured in a 1-cm quartz cuvette using the corresponding pure solvent as a reference. FT-IR Spectrum was acquired using a Nicolet 5700 Fourier transform infrared spectrometer using KBr pellets. Zeta potential measurement was conducted in Zetasizer NanoS from Malvern Instruments. Before the measurement, the particles were directly dispersed in deionized water.

## **Results and discussion**

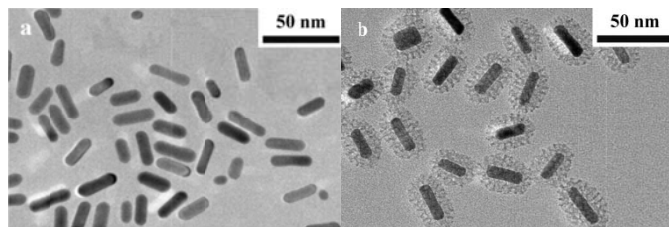


**Fig.1** TEM images of Au nanorod before (a) and after silica coating (b)

Au<sub>rod</sub>@SiO<sub>2</sub> was synthesized by combining the seed-mediated growth and modified stöber method according to the reported method with some modifications,<sup>8</sup> in which CTAB was separately employed as both stabilizing agent for the synthesis of Au nanorods and the soft template for the formation of mesoporous silica shell. Fig.1a gives the representative TEM image of Au nanorods, and it can be seen that the average length and width of Au nanorods are about 30 and 8.5 nm, respectively. After silica coating, the obtained Au<sub>rod</sub>@SiO<sub>2</sub> appears the typical core-shell structure made of a Au

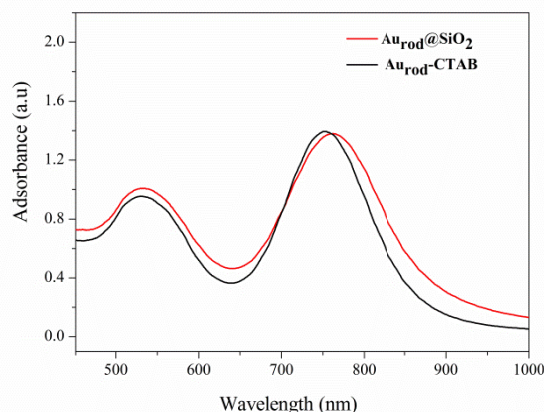


**Fig.2** UV-vis absorbance spectra of Au nanorod and Au<sub>rod</sub>@SiO<sub>2</sub>

nanorod core and uniform silica shell with the average thickness of 11 nm (as shown in Fig.1b), and disordered mesopores can be observed in the silica shell. The corresponding UV-vis absorbance spectra further confirms the successful silica coating of Au nanorods. Fig.2 shows the typical UV-vis absorbance spectra of Au nanorods before and after silica coating. It can be seen that the as-synthesized Au nanorod has a longitudinal surface plasmon resonance (LSPR) peak at 752 nm. After silica shell coating, it only exhibits a red shift of 10 nm, which is well consistent with previous report that the red shift of LSPR peak results from an increase in the local refractive

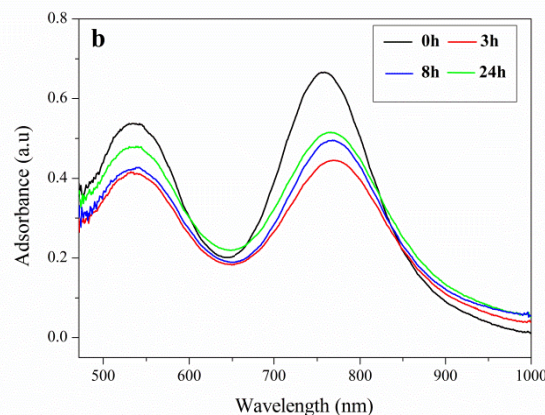
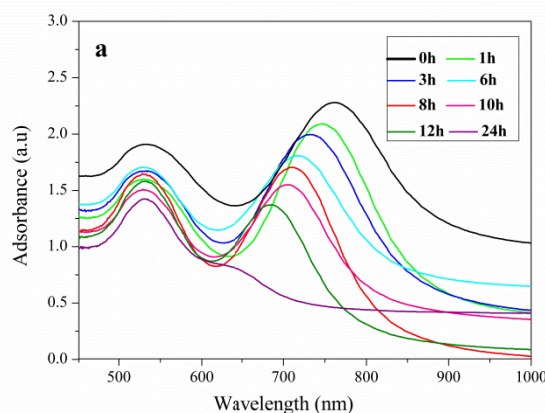


**Fig.3** UV-vis absorbance spectra of Au<sub>rod</sub>@SiO<sub>2</sub> treated by HCl/CH<sub>3</sub>OH (a) extraction at varying stages (0, 1, 3, 6, 8, 10, 12, 24 h) or by NH<sub>4</sub>NO<sub>3</sub>/CH<sub>3</sub>OH (b) extraction at varying stages (0, 3, 8, 24h).

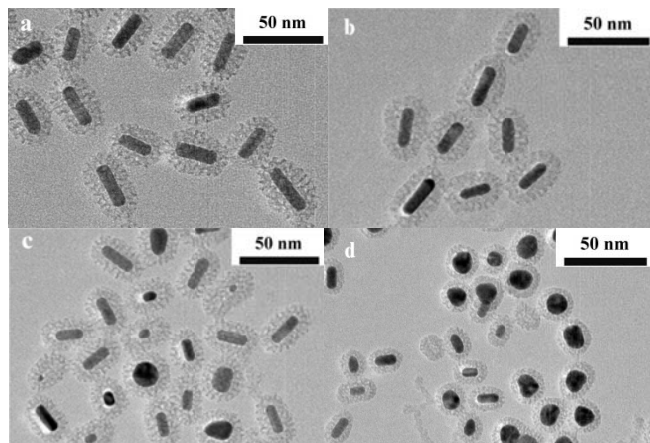


**Fig.4** TEM images of  $\text{Au}_{\text{rod}}@/\text{SiO}_2$  treated by  $\text{HCl}/\text{CH}_3\text{OH}$  extraction at varying stages (a) 0 h; (b) 3 h; (c) 8 h; (d) 24 h

index of the surrounding medium for Au nanorod after replacing CTAB ligands with silica shell.<sup>23</sup> Taking all these above results together, it can be concluded that the typical  $\text{Au}_{\text{rod}}@/\text{SiO}_2$  with core-shell structure is obtained.

As mentioned above, herein we emphatically studied the effect of two kinds of extraction solvents (route A and route B) on both morphology and plasmon-related property of  $\text{Au}_{\text{rod}}@/\text{SiO}_2$ . Fig.3a firstly shows the real-time UV-vis absorbance spectra of the extracted  $\text{Au}_{\text{rod}}@/\text{SiO}_2$  at various stages in route A. In the initial stage of  $\text{HCl}/\text{CH}_3\text{OH}$  extraction,  $\text{Au}_{\text{rod}}@/\text{SiO}_2$  exhibits two adsorption peaks located at 522 and 752 nm, corresponding to the transverse surface plasmon resonance (TSPR) and LSPR, respectively. As the solvent extraction procedure undergoes, the LSPR peak gradually moves to lower wavelength and the corresponding absorbance decreases. When the extraction time is extended to 24 h, the LSPR peak nearly disappears from the absorption spectra and becomes a shoulder of the TSPR peak. Because the LSPR peak is directly determined by the aspect ratio of the Au nanorod, its blue-shift indicates the decrease of the aspect ratio of Au nanorod core and a preferential shortening along the axial direction of the Au nanorod, which is further confirmed by the corresponding TEM images. As shown in Fig.4a, the initial Au nanorod in  $\text{Au}_{\text{rod}}@/\text{SiO}_2$  exhibits an average length of  $30 \pm 3.5$  nm and a width of  $8.6 \pm 0.7$  nm, corresponding to an aspect ratio of 3.50. After 3h extraction, its average length and width are reduced to  $25.0 \pm 3.2$  and  $8.2 \pm 0.4$  nm, respectively, corresponding to an aspect ratio of 3.03, as presented in Fig.4b. When extending the extraction time to 8 h, there is a remarkable shortening in the length of Au nanorods, but little narrowing in width, and the aspect ratio of Au nanorod at this stage decreases from 3.03 to 2.82. At the same time, more spherical Au NPs are observed in Fig.4c. Further extension of the extraction time to 24 h results in the complete shape transformation from the rod-like structure to sphere. As shown in Fig.4d, it can be seen that the initially rod-like outline of the interior Au nanorod almost completely disappeared and became spherical Au particles as cores with the diameter of 22.6 nm. These above results indicate that when  $\text{HCl}/\text{CH}_3\text{OH}$  mixture is used as the extraction solvent, the etching of Au nanorods easily occurs during the removal of CTAB and the shape transformation preferentially occurs along the axial direction of the Au nanorods, which could be attributed to less surface passivation or higher reactivity at the tips of Au nanorods.<sup>17, 18</sup>

As a control, when using  $\text{NH}_4\text{NO}_3/\text{CH}_3\text{OH}$  mixture as extraction solvent in route B, the results are completely different from the above study that no significant shape transformation of  $\text{Au}_{\text{rod}}@/\text{SiO}_2$  can be observed within 24 h. Fig.3b shows the typical UV-vis absorbance spectra of  $\text{Au}_{\text{rod}}@/\text{SiO}_2$  before and after  $\text{NH}_4\text{NO}_3/\text{CH}_3\text{OH}$

extraction. It can be seen that there is only a red shift of 13 nm even we extend the extraction time to 24 h. Moreover, the LSPR peak doesn't show any obvious broadening, suggesting that surfactant removal by  $\text{NH}_4\text{NO}_3/\text{CH}_3\text{OH}$  doesn't induce any obvious shape transformation, which is further confirmed by the corresponding TEM image. As shown in Fig.5, it can be seen that no significant shape transformation of  $\text{Au}_{\text{rod}}@/\text{SiO}_2$  is observed after 24 h extraction in comparison with the original morphology of non-extracted  $\text{Au}_{\text{rod}}@/\text{SiO}_2$  and most of the cores still maintain the rod-like structure.

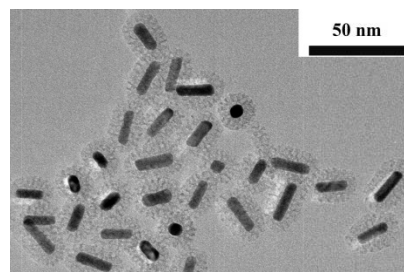


**Fig.5** TEM image of  $\text{Au}_{\text{rod}}@/\text{SiO}_2$  treated by  $\text{NH}_4\text{NO}_3/\text{CH}_3\text{OH}$  extraction for 24 h.

In order to explain the above phenomena, the plausible mechanism is presented as follows: according to Stucky's previous studies,<sup>13</sup> one of main reasons for the shape transformation of Au nanorods is presumably associated with oxidation etching caused by environmentally benign oxygen. And the oxidation rate is controlled by the temperature and acid concentration. According to the Nernst equation of the reduction of  $\text{O}_2$  (see Equation 1),

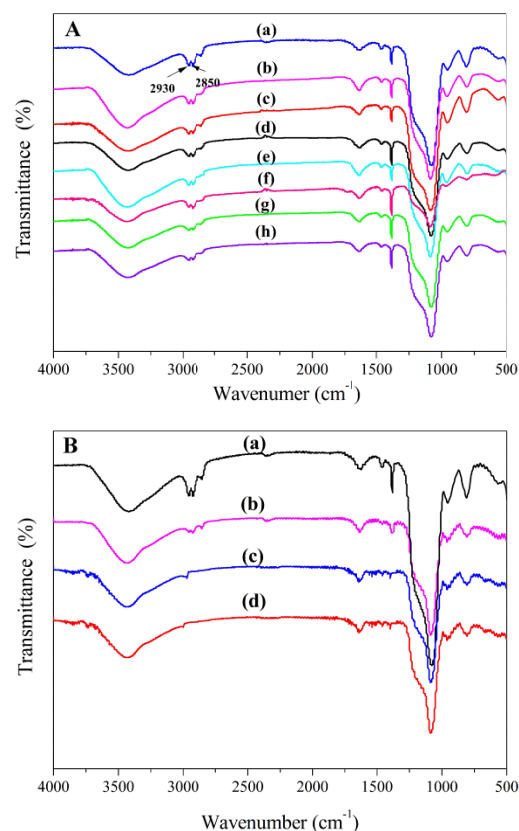
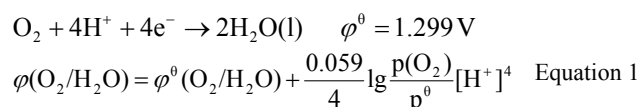


**Fig.6** FT-IR adsorption spectra of  $\text{Au}_{\text{rod}}@/\text{SiO}_2$  before and after different solvent extractions at varying stages. A: by  $\text{HCl}/\text{CH}_3\text{OH}$  solvent (a: before the extraction; b: 1 h; c: 3 h; d: 6 h; e: 8 h; f: 10 h; g: 12 h; h: 24 h); B: by  $\text{NH}_4\text{NO}_3/\text{CH}_3\text{OH}$  solvent (a: before the extraction; b: 3 h; c: 8 h; d: 24 h).



the electrode potential of  $\text{O}_2/\text{H}_2\text{O}$  is proportional to the concentration of  $\text{H}^+$ . In the above experiment, when using  $\text{NH}_4\text{NO}_3/\text{CH}_3\text{OH}$  mixture as extraction solvent, the corresponding pH value of this system is 5.20, i.e., the concentration of  $\text{H}^+$  is about  $10^{-5.2}$  M. As a contrast, the concentration of  $\text{H}^+$  in  $\text{HCl}/\text{CH}_3\text{OH}$  is 0.25 M. Therefore, the oxidative capability of  $\text{O}_2$  for  $\text{HCl}/\text{CH}_3\text{OH}$  is much higher than that for  $\text{NH}_4\text{NO}_3/\text{CH}_3\text{OH}$ , indicating that Au nanorods are easily reshaped in the former case. Moreover, other research also suggests that  $\text{Cl}^-$  from the  $\text{HCl}/\text{CH}_3\text{OH}$  could effectively reduce the electron potential of the gold species,<sup>19</sup> which accelerates the selective etching of elemental gold. In addition, as we know, most of the Au nanorods obtained in the presence of Ag (I) are in the nature of the single crystal grown along (001) direction. The side surfaces are surrounded by (110) and (100) facets, and the tips are enclosed by (111), (110) and (001) facets.<sup>20, 21</sup> Due to the presence of CTAB molecules, (110) and (100) facets become more stable than (111) planes.<sup>22, 23</sup> Therefore, that is why the tips with (111) facets might be preferentially etched in route A. On the other hand, high surface curvature would lead to less passivation of the CTAB molecules at the tip, which also enables the etching reagent ( $\text{HCl}/\text{CH}_3\text{OH}$ ) to more easily approach the tip for the reaction.

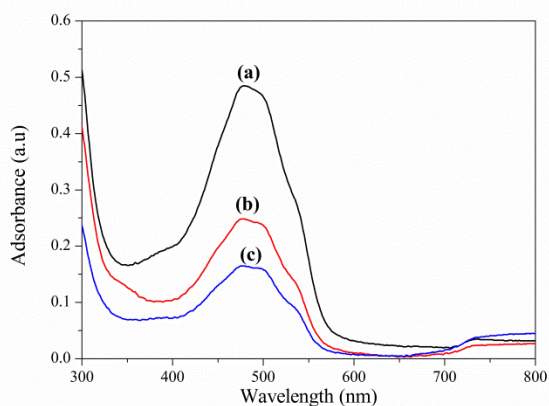


**Fig.7** UV-vis adsorption spectra of the DOX solution before being loaded into  $\text{Au}_{\text{rod}}@\text{SiO}_2$  (a) and after being loaded into the  $\text{Au}_{\text{rod}}@\text{SiO}_2$  treated with  $\text{HCl}/\text{CH}_3\text{OH}$  (b) and with  $\text{NH}_4\text{NO}_3/\text{CH}_3\text{OH}$  (c)

To further evaluate the effect of two extraction solvents on the extraction efficiency of CTAB, FT-IR analysis was conducted to measure the amount of residue CTAB in  $\text{Au}_{\text{rod}}@\text{SiO}_2$  after treatment with the above two extraction solvents. The curve a in Fig.6A shows the FT-IR adsorption spectrum of  $\text{Au}_{\text{rod}}@\text{SiO}_2$  before  $\text{HCl}/\text{CH}_3\text{OH}$  extraction. Two bands at  $\sim 2930$  and  $\sim 2850 \text{ cm}^{-1}$  are due to the asymmetric and symmetric vibrations of  $\text{CH}_2$  units from CTAB molecules, respectively. Therefore, the removal of CTAB could be confirmed by a comparison of the peak absorbance at  $\sim 2930$  or  $\sim 2850 \text{ cm}^{-1}$  during the extraction procedure. As shown in Fig. 6A, after  $\text{HCl}/\text{CH}_3\text{OH}$  extraction for 1 h, the intensity of these  $\text{CH}_2$ -stretching vibration bands slightly weakens. While with the prolongation of extraction time from 1 to 24 h, no obvious decrease is seen for the intensity of 2930 and 2850  $\text{cm}^{-1}$  band, indicating that there is still some residual CTAB inside the mesopore of siliceous framework. However, when using  $\text{NH}_4\text{NO}_3/\text{CH}_3\text{OH}$  mixture as extraction solvent, as shown in Fig.6B, it can be seen that the intensity of those two  $\text{CH}_2$ - stretching vibration bands significantly decrease as the extraction time reaches 8 h, which implies that most of CTAB has been successfully extracted. When the extraction time is extended to 24 h, both of  $\text{CH}_2$ - stretching vibration bands almost

disappear, suggesting that CTAB has been completely removed from  $\text{Au}_{\text{rod}}@\text{SiO}_2$ . As mentioned above, the purpose of introduction of  $\text{NH}_4\text{NO}_3$  or  $\text{HCl}$  in methanol is to break the electrostatic force between the oligomeric silicate anions and cationic headgroups ( $\text{CTA}^+$ ) of the CTAB. According to the previous study,<sup>24</sup> the  $\text{NH}_4^+$  ion can directly spread to the internal mesopore of siliceous framework and exchange with the  $\text{CTA}^+$  due to a weak interaction between the  $\text{NH}_4^+$  ions and  $\text{SiO}^-$  groups at the surface of the mesopore, followed with the consequent desorption of ammonia from the extracted samples, which is probably generated by heating  $\text{NH}_4^+$  ions in the  $\text{Au}_{\text{rod}}@\text{SiO}_2$ . So such behavior allows more  $\text{NH}_4^+$  ions to further exchange with  $\text{CTA}^+$  as long as there are CTAB molecules left inside the mesopore of  $\text{Au}_{\text{rod}}@\text{SiO}_2$ . As a control, ion exchange rate between  $\text{H}^+$  and  $\text{CTA}^+$  has been reported to be comparatively slower, therefore decreasing the extraction efficiency of CTAB. In addition, the structure transformation of  $\text{Au}_{\text{rod}}@\text{SiO}_2$  during the solvent extraction may be also presumably responsible for the lower extraction efficiency of CTAB removal considering the fact that the reshaped Au nanorod in the inner core could block the channel for the free spread of proton, which further makes the ion exchange between proton and  $\text{CTA}^+$  even more difficult.

As previously stated in the introduction section, one of the potential applications of  $\text{Au}_{\text{rod}}@\text{SiO}_2$  is to be used as drug carrier. Therefore, we further investigate the effect of two extraction solvents on the drug loading capacity of the resulting  $\text{Au}_{\text{rod}}@\text{SiO}_2$ . Fig.7 gives the UV-vis adsorption spectra of the original DOX solution (a), the residual DOX solution after being absorbed by  $\text{Au}_{\text{rod}}@\text{SiO}_2$  treated with  $\text{HCl}/\text{CH}_3\text{OH}$  (b) or with  $\text{NH}_4\text{NO}_3/\text{CH}_3\text{OH}$  (c), respectively. It can be seen that the adsorption intensity of DOX decrease greatly after interaction with  $\text{Au}_{\text{rod}}@\text{SiO}_2$ ,

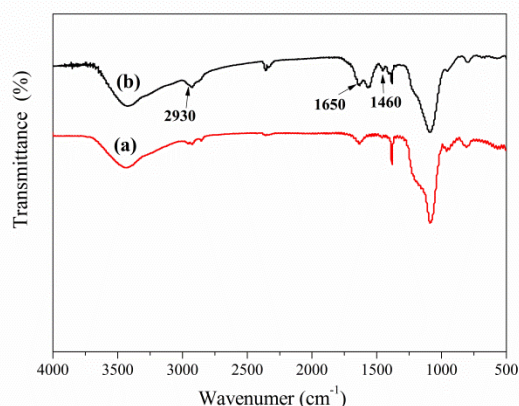


**Fig.8** FT-IR spectra of  $\text{Au}_{\text{rod}}@\text{SiO}_2$  after  $\text{NH}_4\text{NO}_3/\text{CH}_3\text{OH}$  extraction (a) and PEGylated  $\text{Au}_{\text{rod}}@\text{SiO}_2$  (b).

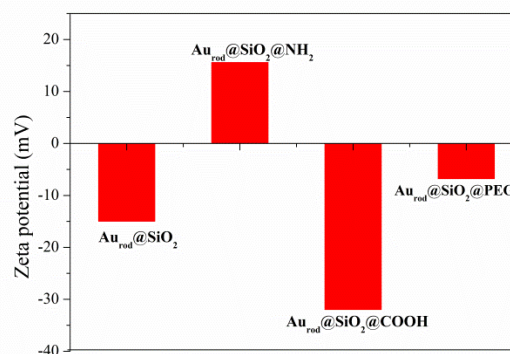


**Fig.9** Zeta potential of  $\text{Au}_{\text{rod}}@\text{SiO}_2$ ,  $\text{Au}_{\text{rod}}@\text{SiO}_2@\text{NH}_2$ ,  $\text{Au}_{\text{rod}}@\text{SiO}_2@\text{COOH}$  and  $\text{Au}_{\text{rod}}@\text{SiO}_2@\text{PEG}$ .

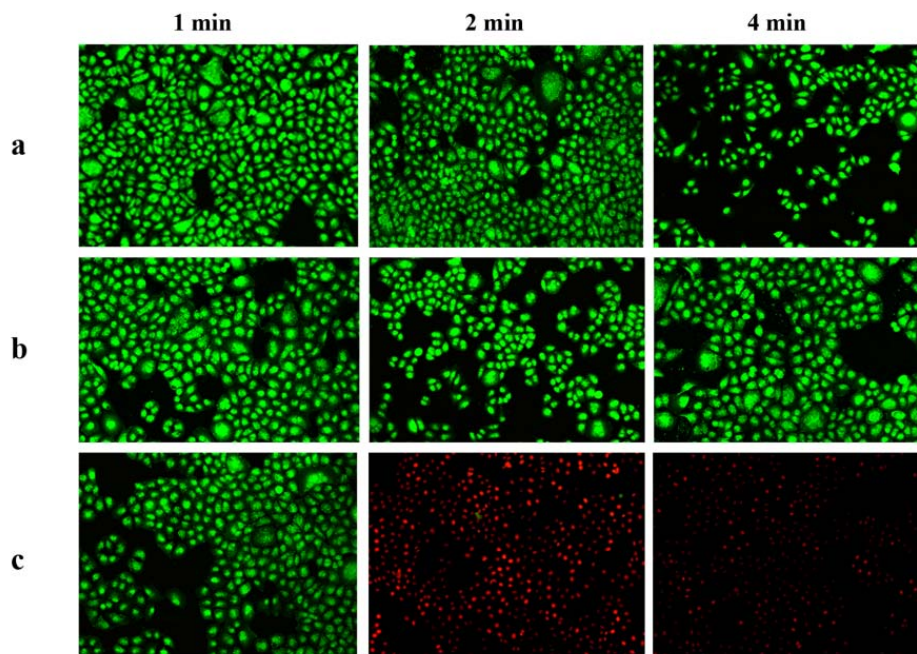


**Fig.10** Fluorescence images of Calcein-AM/propidium iodide co-stained YCC-2 cells after the same PTT treatment. a: control experiment, without the addition of any  $\text{Au}_{\text{rod}}@ \text{SiO}_2$ ; b: YCC-2 cells incubated with  $\text{Au}_{\text{rod}}@ \text{SiO}_2$  treated with  $\text{HCl}/\text{CH}_3\text{OH}$  extraction; c: YCC-2 cells incubated with  $\text{Au}_{\text{rod}}@ \text{SiO}_2$  treated with  $\text{NH}_4\text{NO}_3/\text{CH}_3\text{OH}$  extraction.

indicating that DOX molecules can be loaded into  $\text{Au}_{\text{rod}}@ \text{SiO}_2$ . Further comparison between  $\text{Au}_{\text{rod}}@ \text{SiO}_2$  treated with different extraction solvents shows that  $\text{Au}_{\text{rod}}@ \text{SiO}_2$  treated with  $\text{NH}_4\text{NO}_3/\text{CH}_3\text{OH}$  possesses a larger drug loading capacity than that treated with  $\text{HCl}/\text{CH}_3\text{OH}$ . According to the decrement of absorbance of DOX, the loading efficiency of  $\text{Au}_{\text{rod}}@ \text{SiO}_2$  treated with  $\text{NH}_4\text{NO}_3/\text{CH}_3\text{OH}$  and  $\text{HCl}/\text{CH}_3\text{OH}$  reach 82.5% and 71.1%, respectively. Such loading efficiency difference may be explained as follows: firstly,  $\text{NH}_4\text{NO}_3/\text{CH}_3\text{OH}$  extraction route possesses higher extraction efficiency, therefore leading to more open internal channel after the removal of CTAB, which in turn results in an enhanced drug loading capacity. Secondly, the long-time extraction with  $\text{HCl}/\text{CH}_3\text{OH}$  would undoubtedly cause the non-negligible pore contraction, which also leads to a poorer drug loading capacity compared with samples treated with  $\text{NH}_4\text{NO}_3/\text{CH}_3\text{OH}$ . So it can be expected that  $\text{Au}_{\text{rod}}@ \text{SiO}_2$  treated with  $\text{NH}_4\text{NO}_3/\text{CH}_3\text{OH}$  would possess much larger drug loading capacity than that treated with  $\text{HCl}/\text{methanol}$ .

To further improve the biocompatibility of  $\text{Au}_{\text{rod}}@ \text{SiO}_2$  to be used for photo-thermal therapy, their surface was also functionalized with  $\alpha$ -mPEG- $\omega$ -amine group. Fig.8 gives the FT-IR adsorption spectra of  $\text{Au}_{\text{rod}}@ \text{SiO}_2$  (a) and PEGylated  $\text{Au}_{\text{rod}}@ \text{SiO}_2$  (b), respectively, it can be seen that after the linkage of PEG group to the surface of  $\text{Au}_{\text{rod}}@ \text{SiO}_2$ , the  $\text{Au}_{\text{rod}}@ \text{SiO}_2@ \text{PEG}$  shows the typical C-H mode at  $2850\sim 2930\text{ cm}^{-1}$  and  $1462\text{ cm}^{-1}$ , which should be associated with C-H bonds in the PEG block. In addition, a peak at  $1650\text{ cm}^{-1}$  can be assigned to the amide carbonyl groups, indicating the successful linkage of mPEG<sub>10000</sub>-NH<sub>2</sub> to the surface of  $\text{Au}_{\text{rod}}@ \text{SiO}_2@ \text{COOH}$  via amidation reaction. In order to further track the evolution of linked groups on the surface of  $\text{Au}_{\text{rod}}@ \text{SiO}_2$ , the zeta potential characterization was also conducted. As shown in Fig.9, the zeta potential of  $\text{Au}_{\text{rod}}@ \text{SiO}_2$  is  $-15.6\text{ mV}$  before APTES functionalization, showing the existence of a lot of silanol groups. Meanwhile, amine-functionalized  $\text{Au}_{\text{rod}}@ \text{SiO}_2$  presents a positive zeta potential of  $+15.6\text{ mV}$ . After grafting with

PAA, the potential of  $\text{Au}_{\text{rod}}@ \text{SiO}_2@ \text{COOH}$  decreases to  $-32.0\text{ mV}$ , indicating the existence of a great amount of carboxyl groups on the surface of PAA modified  $\text{Au}_{\text{rod}}@ \text{SiO}_2$ . As an evidence for the successful conjugation of mPEG<sub>10000</sub>-NH<sub>2</sub>, the zeta potential of  $\text{Au}_{\text{rod}}@ \text{SiO}_2@ \text{PEG}$  increases from  $-32.0$  to  $-6.0\text{ mV}$ , suggesting that most of carbonyl groups from the surface of  $\text{Au}_{\text{rod}}@ \text{SiO}_2@ \text{COOH}$  have reacted with mPEG<sub>10000</sub>-NH<sub>2</sub>. Taking all the above results together, it can be concluded that PEGylated  $\text{Au}_{\text{rod}}@ \text{SiO}_2$  is obtained.

Finally, we studied the enhanced *in vitro* photo-thermal therapy efficiency of  $\text{Au}_{\text{rod}}@ \text{SiO}_2$  after treatment with two extraction solvents by Calcein-AM/Propidium iodide double staining assay. As we know, Calcein AM, a live cell stain, is a nonfluorescent dye that can permeate the cell membrane and be further hydrolyzed by intracellular esterases to a green fluorescent calcein dye in live cells. Propidium iodide, a dead cell staining, is membrane nonpermeable and generally excluded from viable cells. And it can bind to the DNA of dead cells by intrabase intercalation, generating red fluorescence.<sup>25</sup> Fig.10a gives the fluorescence images of negative control after irradiation at selected time (1, 2, 4 min), all the YCC-2 cells remain healthy with green calcein fluorescence even we extend the irradiation time to 4 min, suggesting that 808 laser irradiation alone is not harmful for cells. However, remarkably enhanced cancer cell killing efficiency can be observed for the YCC-2 cells cultured with PEGylated  $\text{Au}_{\text{rod}}@ \text{SiO}_2$  treated with  $\text{NH}_4\text{NO}_3/\text{CH}_3\text{OH}$  (Fig.10c) when the irradiation time is 2 min. As a control, the same light irradiation induces no cellular damage for cells cultured with PEGylated  $\text{Au}_{\text{rod}}@ \text{SiO}_2$  treated with  $\text{HCl}/\text{CH}_3\text{OH}$  (Fig.10b) even we extend the irradiation time to 4 min. Such cancer killing efficiency difference can be explained as follows:  $\text{Au}_{\text{rod}}@ \text{SiO}_2$  treated with  $\text{NH}_4\text{NO}_3/\text{CH}_3\text{OH}$  well maintains the original structure of Au nanorod, whereas the original structure of Au nanorod in  $\text{Au}_{\text{rod}}@ \text{SiO}_2$  is completely damaged when treated with  $\text{HCl}/\text{CH}_3\text{OH}$ . Therefore, photo-thermal conversion efficiency of the  $\text{Au}_{\text{rod}}@ \text{SiO}_2$  treated with  $\text{NH}_4\text{NO}_3/\text{CH}_3\text{OH}$  is greater than

that treated with HCl/CH<sub>3</sub>OH, which in turn leads to an enhanced cancer cells killing efficiency. Our results collectively demonstrate that the selection of extraction solvent for the removal of CTAB from Au<sub>rod</sub>@SiO<sub>2</sub> could have great impact on its photothermal conversion property, which further influences its efficacy as a theranostic platform.

## Conclusions

In summary, this paper emphatically studied the effect of template removal on both the morphology of Au<sub>rod</sub>@SiO<sub>2</sub> and its biomedical application such as drug loading and in vitro photo-thermal therapy. And we have found that when using NH<sub>4</sub>NO<sub>3</sub>/CH<sub>3</sub>OH as the extraction solvent it only takes 8 h to remove most of CTAB from the pores of Au<sub>rod</sub>@SiO<sub>2</sub> without damaging the morphology of the internal Au nanorod. And the LSPR of Au nanorod doesn't show any obvious peak broadening after the extraction. However, Au<sub>rod</sub>@SiO<sub>2</sub> treated with HCl/CH<sub>3</sub>OH suffers from both poor extraction efficiency and shape transformation of the internal Au nanorod, which is presumably associated with oxidation etching during the extraction. After 24 h extraction in this case, the LSPR peak of Au nanorods nearly disappears from the absorption spectra and becomes a shoulder of the TSPR peak. The consequent drug loading experiment shows that Au<sub>rod</sub>@SiO<sub>2</sub> treated with NH<sub>4</sub>NO<sub>3</sub>/CH<sub>3</sub>OH has a larger drug loading capacity than that treated with HCl/CH<sub>3</sub>OH, with a loading efficiency of 82.5%. Furthermore, the in vitro photo-thermal therapy experiment shows that Au<sub>rod</sub>@SiO<sub>2</sub> treated with NH<sub>4</sub>NO<sub>3</sub>/CH<sub>3</sub>OH is much more efficient in killing the YCC-2 gastric cancer cells as compared with that extracted by HCl/CH<sub>3</sub>OH. All these above results have laid a solid foundation for the application of Au<sub>rod</sub>@SiO<sub>2</sub> in both photo-thermal therapy and drug delivery.

## Acknowledgements

This work was supported by the State key Basic Research Program of the PRC (2014CB744501, 2010CB933903), and the NSF of China (61271056).

## Notes and references

<sup>a</sup> School of Chemistry and Chemical Engineering, Southeast University, Nanjing, 211189, China. Email: zfwang@seu.edu.cn

<sup>b</sup>School of Biological Science and Medical Engineering, Southeast University, Nanjing, 210096, China. Email: nyhe1958@163.com

- G. Kickelbick, *In Hybrid Materials: Synthesis, Characterisation and Applications*, Wiley-VCH: Weinheim, Germany, 2007.
- Z. Wang, S. Zong, J. Yang, J. Li and Y. Cui, *Biosens. Bioelectron.*, 2011, **26**, 2883.
- J. Qian, L. Jiang, F. Cai, D. Wang and S. He, *Biomaterials*, 2011, **32**, 1601.
- D. K. Yi, I. C. Sun, J. H. Ryu, H. Koo, C. W. Park, I. C. Youn, K. Choi, I. C. Kwon, K. Kim and C. H. Ahn, *Bioconjug. Chem.*, 2010, **21**, 2173.
- T. B. Huff, L. Tong, Y. Zhao, M. N. Hansen, J.-X. Cheng and A. Wei, *Nanomedicine*, 2007, **2**, 125.
- W. X. Mai and H. Meng, *Integr. Biol.*, 2013, **5**, 19.
- Y. Chen, H. Chen and J. Shi, *Adv. Mater.*, 2013, **25**, 3144.
- I. Gorelikov and N. Matsuura, *Nano Lett.*, 2008, **8**, 369.
- M. T. Keene, R. D. Gougeon, R. Denoyel, R. K. Harris, J. Rouquerol and P. L. Llewellyn, *J. Mater. Chem.*, 1999, **9**, 2843.
- C. Urata, Y. Aoyama, A. Tonegawa, Y. Yamauchi and K. Kuroda, *Chem. Commun.*, 2009, **34**, 5094.
- H. Ji, Y. Fan, W. Jin, C. Chen and N. Xu, *J. Non-Cryst. Solids*, 2008, **354**, 2010.
- N. R. Jana, L. Gearheart, S. O. Obare and C. J. Murphy, *Langmuir*, 2002, **18**, 922.

- C.-K. Tsung, X. Kou, Q. Shi, J. Zhang, M. H. Yeung, J. Wang and G. D. Stucky, *J. Am. Chem. Soc.*, 2006, **128**, 5352.
- R. Zou, X. Guo, J. Yang, D. Li, F. Peng, L. Zhang, H. Wang and H. Yu, *CrystEngComm*, 2009, **11**, 2797-2803.
- T. Sreepasad, A. Samal and T. Pradeep, *Langmuir*, 2007, **23**, 9463.
- B. Van de Broek, N. Devoogdt, A. D'Hollander, H.-L. Gijs, K. Jans, L. Lagae, S. Muyltermans, G. Maes and G. Borghs, *ACS nano*, 2011, **5**, 4319.
- S. Link, M. Mohamed and M. El-Sayed, *J. Phys.Chem. B*, 1999, **103**, 3073.
- K. Caswell, J. N. Wilson, U. H. Bunz and C. J. Murphy, *J. Am. Chem. Soc.*, 2003, **125**, 13914.
- J. A. Dean, *Lange's Handbook of Chemistry*, 15th edn., McGraw-Hill, 1999.
- Y. Xiang, X. Wu, D. Liu, L. Feng, K. Zhang, W. Chu, W. Zhou and S. Xie, *J. Phys. Chem. C*, 2008, **112**, 3203.
- X. Kou, S. Zhang, C. K. Tsung, Z. Yang, M. H. Yeung, G. D. Stucky, L. Sun, J. Wang and C. Yan, *Chem. Eur. J.*, 2007, **13**, 2929.
- R. T. Tom, A. Samal, T. Sreepasad and T. Pradeep, *Langmuir*, 2007, **23**, 1320.
- C. J. Johnson, E. Dujardin, S. A. Davis, C. J. Murphy and S. Mann, *J. Mater. Chem.*, 2002, **12**, 1765.
- N. Lang and A. Tuel, *Chem. Mater.*, 2004, **16**, 1961.
- D. K. Kirui, D. A. Rey and C. A. Batt, *Nanotechnology*, 2010, **21**, 105105.